

A Parametric Study of L-shape Coaxial Closed-Loop Geothermal Systems with Reservoir Convection

Gabriela Bran Anleu¹, Raquel S.P. Hakes¹, Radoslav Bozinoski¹, Koenraad Beckers²

¹Sandia National Laboratories, Livermore, CA, USA

²National Renewable Energy Laboratory, Golden, CO, USA

Keywords: Closed-loop geothermal, advanced geothermal systems, reservoir simulations, reservoir convection, coaxial geothermal systems

ABSTRACT

Closed-loop geothermal systems (CLGS) have become of interest because they do not require reservoir permeability, which may increase the number of sites where they can be utilized. In addition, the working fluid is constantly recirculated and therefore conserved. This gives the flexibility of selecting different working fluids, such as water and supercritical CO₂, which can directly drive a turbine for generating electricity. However, for conduction-only reservoirs, CLGS require deep wellbores and long laterals to overcome the limited heat transfer area. This may not be feasible due to the geothermal location or the cost of drilling. To enhance the heat extraction, wet-rock geothermal systems have been proposed. This idea suggests that the convection (either natural or forced) in the porous rock will improve the heat extraction of the system by flow of in-situ water in the reservoir. Previous work has shown that natural convection can improve the performance of the geothermal systems with U-tube configuration, but only in cases of high reservoir permeability. In this work, we developed a numerical model for a wet-rock CLGS with a coaxial configuration where liquid convection is allowed in the rock. We then compared the heat extracted from the dry rock coaxial CLGS and the wet rock U-tube CLGS to determine if there are any advantages to having convection in the coaxial configuration. The effects on performance of working fluid mass flow rate, permeability, and geothermal temperature gradient in the reservoir have been investigated. The advantage of natural convection highly depends on the permeability and the geothermal temperature gradient. The U-tube system performs better than the L-shape coaxial system.

1. INTRODUCTION

Closed-loop geothermal (CLG) represents geothermal systems where the heat transfer fluid stays within the wellbore heat exchanger, in contrast to traditional hydrothermal systems or enhanced geothermal systems, where the heat transfer fluid flows through the rock matrix, or natural or man-made fractures of the host formation. CLG has recently received significant interest as a next-generation geothermal technology. For CLG designs relying on heat conduction-only in the reservoir, no reservoir permeability is required, opening areas for development beyond traditional geothermal settings. However, the thermal performance of such systems is dependent on the total heat transfer area of the heat exchanger, requiring tens of kilometers of drilling length to produce multi-MWe output. Other designs have been proposed where convection in the reservoir is leveraged to enhance the thermal output of the CLG system. In a previous study, we studied U-tube type systems subject to convection (Hakes et al. 2024). In this study, we investigate impact of convection on thermal performance of co-axial systems with a horizontal extent.

This study is part of a suite of analysis performed by the Closed-Loop Geothermal Working Group, a DOE-funded research initiative launched in 2021 and involving multiple national laboratories and universities studying the techno-economic performance of various closed-loop geothermal designs. Initial efforts focused on U-tube and co-axial systems in conduction-only reservoirs (White et al., 2024). A web-based tool, GeoCluster, was created to allow users to run their own simulations (Beckers et al. 2023). Other efforts as part of the CLGWG include analyzing performance of thermal enhancements (Beckers, Ketchum, and Augustine 2024) and dispatchable closed-loop geothermal operation (Aljubran and Horne 2025).

In this work, we present the impacts of changing permeability, geothermal gradient, and mass flow rate of the working fluid on the heat extraction of a coaxial system. We highlight the advantages of having natural convection in the formation versus having convection-only. We compare the effectiveness of the coaxial system with a U-tube closed-loop system under analogous conditions.

2. METHODS

Three-dimensional simulations were conducted for both a U-tube configuration described in (Hakes et al. 2024) and an L-shaped coaxial configuration described in (White et al., 2024) of a CLGS. For both configurations, the vertical segments are assumed to be in a conduction-only reservoir while the horizontal segments are in a convective reservoir. All simulations are conducted in Sierra Thermal/Fluids code, Aria, a multiphysics finite element code developed at Sandia National Laboratories ("SIERRA Multimechanics Module: Aria User Manual (V.5.6)" 2022). Temperature as a function of time and heat output at 20 years are compared for varying permeability, geothermal gradient, and mass flow rate of the working fluid.

2.1 Numerical Domain

Figure 1 shows the side and top view of the coaxial L-shape geothermal system being modeled. The side view shows a coaxial L-shape tube with a vertical section of length $L_V = 2500$ m and a horizontal section of length $L_H = 1000$ m. As shown in the top view, the coaxial tube, which is inserted into a borehole of diameter $D_3 = 0.4445$ m, has an area ratio (annular area/pipe area) of 1 and an inner pipe wall thickness of 19.2 mm. The coaxial tube in the vertical section is surrounded by hot dry rock (HDR) of diameter $D_4 = 350$ m. The coaxial tube in the horizontal section is surrounded by a layer of permeable hot wet rock (HWR) with a thickness of 100 m. The permeable HWR is sandwiched between an over- and underburden of impermeable HWR with a thickness of 62.5 m and a very low permeability of 0.001 mD. The vertical HDR formation is decoupled from the horizontal HWR formation, except through heat exchange with the circulating fluid. The descending working fluid is coupled to the ascending working fluid at the end of the horizontal section by enforcing the temperature to be equal. The mesh is biased towards the borehole to resolve the radial temperature gradients. The mesh resulted in 1,553,084 nodes. The model was run in parallel using 244 processors.

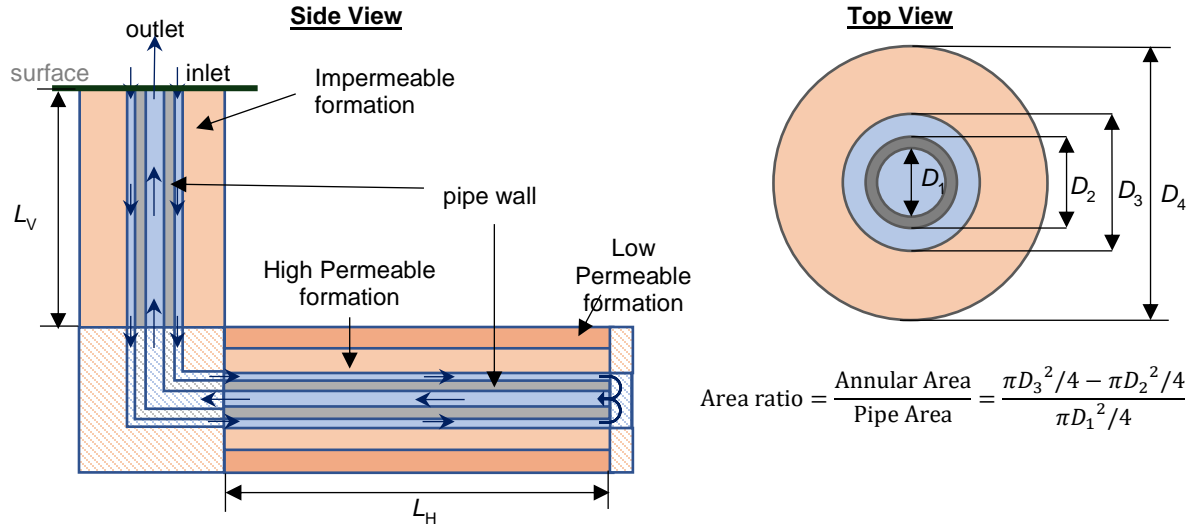


Figure 1: Side and top view of coaxial L-shape geothermal system being modeled with a vertical HDR section and a horizontal HWR section. The HWR consists of a section with high permeability sandwiched in a low permeability section. The shaded elbow and shaded recirculation section are not included in the model.

The working fluid, in this case liquid water, is injected into the annulus at 30 °C and 20 MPa at a constant mass flow rate, and it returns in the inner pipe. The density, specific heat capacity, thermal conductivity, and viscosity of the water are a function of pressure and temperature and are obtained using CoolProps (Bell et al. 2014). The wall pipe between the annulus and inner pipe is assumed to have a very low thermal conductivity of 0.06 W/m-K to reduce the heat transfer between the working fluid as it descends the annulus and returns up the inner pipe. To minimize the heat capacity of the wall, the density and specific heat of the wall were assumed to be 1 kg/m³ and 1 J/kg-K, respectively. The HDR has a density of 2750 kg/m³, a specific heat of 790 J/kg-K, and a thermal conductivity of 3.05 W/m-K. The HWR has a solid density of 2750 kg/m³ with a porosity of 0.1, a specific heat of 790 J/kg-K, and a thermal conductivity of 3.05 W/m-K. The temperature at the surface was kept at 25°C. We varied the geothermal temperature gradient, the HWR permeability, and the working fluid mass flow rate. Table 1 summarizes the material properties used in the model. The properties that we varied are in bold.

We are also interested in comparing the performance of the coaxial system with the U-tube system. Previous work (Hakes et al. 2024) investigated the impact of convection on U-tube systems. For the comparison, we used the same system conditions: the vertical sections and the horizontal section of the U-tube system have the same vertical length (L_V) and horizontal length (L_H) of the coaxial, respectively. The U-tube system also uses HDR for the vertical sections, and HWR for the horizontal section. The borehole diameter is also the same, although the cross-sectional area for the descending and ascending working fluid is smaller for the coaxial system. Thermal properties for water, the HDR, and the HWR are also the same.

2.2 Parameter space

We investigated two mass flow rates of the working fluid: 2 kg/s and 10 kg/s, the permeability of the rock (1 mD - 5 D), and the geothermal gradient within the rock (30 °C/km, 60 °C/km, and 90 °C/km). The lower permeability values are selected to match what is seen in various well locations. The upper values are selected to determine what conditions are needed to see a significant impact of convection, as well as to compare with previous work on U-tube configurations (Hakes et al. 2024). The geothermal gradient range is consistent with typical values found within the first few kilometers' depth of the crust.

Table 1: Material properties for the different components in the L-shape coaxial system.

	HDR	HWR	Impermeable HWR	Pipe Wall	Working fluid
Density (kg/m^3)	2750	2750	2750	1	$f(T,P)$
Specific heat (J/kg-K)	790	790	790	1	$f(T,P)$
Thermal conductivity (W/m-K)	3.05	3.05	3.05	0.06	$f(T,P)$
Viscosity (Pa-s)	-	-	-	-	$f(T,P)$
Porosity (-)	-	0.1	0.1	-	-
Pipe roughness (m)	-	-	-	2.5e-05	-
Permeability (D)	-	0.001 – 5	1e-6	-	-
Geothermal temperature gradient ($^\circ\text{C/km}$)	30, 60, or 90	30, 60, or 90	30, 60, or 90	-	-
Mass flow rate (kg/s)	-	-	-	-	2 or 10

2.3 Governing Equations

2.3.1 Heat transfer model for Working Fluid

The governing equations for the descending and ascending working fluid are simplified to an area-averaged 1D model. The continuity equation assumes a constant mass flow rate. For the conservation of momentum, a balance between the working fluid pressure, P_{wf} , the gravitational forces, F_b , and the wall shear stress, τ_w , is:

$$\int \frac{\partial P_{wf}}{\partial z} d\Omega = \int F_b d\Omega - \int \tau_w d\Gamma \quad (1)$$

The wall shear stress is calculated using the Darcy-Weisbach friction factor formulation (Incropera et al. 1996),

$$\tau_w = \frac{1}{8} f \rho_{wf} u_{wf}^2 \quad (2)$$

where ρ_{wf} and u_{wf} are the density and velocity of the working fluid. The friction factor, f , is calculated using the Haaland correlation (Munson, Young, and Okiishi 1995),

$$\frac{1}{\sqrt{f}} = -1.8 \log \left[\left(\frac{\varepsilon/D}{8} \right)^{1.11} + \frac{6.9}{Re} \right] \quad (3)$$

where ε is the effective roughness height of the pipe, D the pipe inner diameter, $Re_{D_H} = \frac{\rho_{wf} u_{wf} D_H}{\mu_{wf}}$ is the Reynolds number which uses the dynamic viscosity, μ_{wf} .

The working fluid temperature, T_{wf} , is assumed to be constant in the radial direction, and it is calculated using the energy equation:

$$\rho_{wf} c_{p,wf} \frac{\partial T_{wf}}{\partial t} + \rho_{wf} c_{p,wf} u_{wf} \frac{\partial T_{wf}}{\partial z} = h_s (T_{wf} - T_s) \quad (4)$$

where $c_{p,wf}$ is the specific heat of the working fluid, T_s is the temperature of the formation or the pipe wall surface, and h_s is the convective heat transfer coefficient between the surface of the formation or pipe walls and the working fluid, and is defined as,

$$h_s = \frac{k_{wf} Nu}{D_H} \quad (5)$$

where $D_H \equiv 4A_c/P$ is the hydraulic diameter of either the pipe or the annular with a flow cross-sectional area, A_c , and a wetted perimeter, P . Nu is the Nusselt number, which is calculated using the Gnielinski correlation for turbulent flows in pipes (Incropera et al. 1996),

$$Nu = \frac{f/8 (Re_{D_H} - 1000) Pr}{1 + 12.7 (f/8)^{1/2} (Pr^{2/3} - 1)} \quad (6)$$

where $Pr = \frac{\nu_{wf}}{\alpha_{wf}}$ is the Prandtl number, which is the ratio of the kinematic viscosity, ν_{wf} , and thermal diffusivity, α_{wf} , of the working fluid.

2.3.2 Heat transfer model for HDR and pipe wall

The temperature of the HDR is calculated from the energy equation

$$\frac{\partial(\bar{\rho}c_{p,s}\bar{T})}{\partial t} = -\frac{\partial q_j^h}{\partial x_j} \quad (7)$$

The energy diffusive flux vector, q_j^h , is given by Fourier's Law,

$$q_j^h = -\kappa \frac{\partial \bar{T}}{\partial x_j} \quad (8)$$

where κ is the thermal conductivity of the rock.

2.3.3 Heat transfer model for HWR

The horizontal permeable region is a porous formation saturated with liquid water. Natural convection is allowed in the porous region. The liquid and solid phases in the permeable region are assumed to be at the same temperature, T_p . The porous enthalpy equation within the porous region is solved for T_p using the enthalpy, $h_\beta = c_{p,\beta}T_p$, where β represents the phase, either liquid or solid,

$$\frac{\partial}{\partial t}[(\phi - 1)\rho_s h_s + \phi\rho_l h_l] + \frac{\partial(\rho_l u_{jl} h_l)}{\partial x_j} = -\frac{\partial q_j^{hl}}{\partial x_j} - \frac{\partial q_j^{hs}}{\partial x_j} \quad (9)$$

where q_j^{hl} is the liquid phase energy flux,

$$q_j^{hl} = -\phi\rho_l D_l \frac{\partial h_l}{\partial x_j} \quad (10)$$

where D_l is the mixture averaged liquid phase mass diffusivity. The solid phase energy diffusive flux vector, q_j^{hs} , is given by Fourier's Law,

$$q_j^{hs} = -\kappa \frac{\partial T_p}{\partial x_j} \quad (11)$$

where κ is the thermal conductivity of the solid phase. The velocity of the liquid phase, u_{jl} , is calculated using the Darcy approximation in the j -direction, which approximates the momentum equation,

$$u_{jl} = -\frac{\bar{K}}{\mu_l} \left(\frac{\partial p_l}{\partial x_j} + \rho_l g_j \right) \quad (12)$$

where \bar{K} is the mixture averaged solid phase permeability tensor, μ_l is the liquid phase viscosity, and g_j is the gravity vector in the j -direction.

The pressure of the liquid phase, p_l , is solved from the mass balance equation for the liquid phase,

$$\frac{\partial(\phi\rho_l)}{\partial t} + \frac{\partial(\rho_l u_{jl})}{\partial x_j} = \frac{\partial(\phi\rho_l)}{\partial t} - \frac{\partial \left(\rho_l \frac{\bar{K}}{\mu_l} \left(\frac{\partial p_l}{\partial x_j} + \rho_l g_j \right) \right)}{\partial x_j} = 0 \quad (13)$$

where ϕ is the solid phase porosity, and $\rho_l(T_p, p_l)$ is the liquid density.

3. RESULTS

In Section 3.1, we present the results obtained for the coaxial system. We are specifically interested in the outlet temperature at the surface and the thermal energy as a function of time and how these change with mass flow rate (2 kg/s and 10 kg/s), geothermal temperature gradient (30 °C/km, 60 °C/km, and 90 °C/km), and permeability (1 mD – 5 D). The improvement due to convection, if any, will be highlighted. In Section 3.2, we compare the results from the L-shape coaxial model and the U-tube model.

3.1 Coaxial systems

The rock and fluid temperature in the HDR and the HWR after 20 years of operation are shown in Figure 2. These results are for a mass flow rate of 10 kg/s, a permeability of 1 D, and a temperature gradient of 30 °C/km. The cold working fluid heats up as it flows down the annular tube by removing heat from the HDR. A radial temperature gradient forms on the HDR where temperature is highest away from the coaxial tube and gradually decreases as you move closer towards the coaxial tube. The working fluid continues to heat up in the HWR horizontal section. Convection cells formed on the horizontal section due to the heat exchange between the HWR and the working fluid,

as shown in Figure 2. Cooled, denser formation water at the edge of the coaxial tube induces a downward flow near the coaxial tube pushing the hotter formation water upwards, resulting in a pair of counter-rotating buoyancy driven convection cells. A maximum velocity of $2.6e^{-7}$ m/s is observed at the edge of the coaxial tube, and far away from the coaxial tube, the velocity is almost negligible ($3.2e^{-8}$ m/s). By increasing the HWR geothermal temperature gradient, the HWR permeability, or the mass flow rate of the working fluid, the convective velocity of the formation water increases.

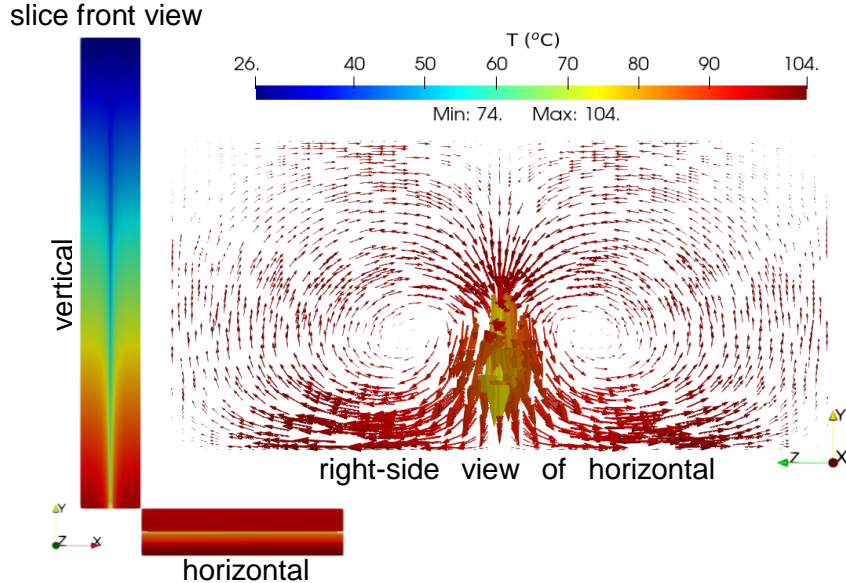


Figure 2: Slice front view showing the temperature gradient after 20 years of operations and right-side view of horizontal section showing the buoyantly driven convection cells on either side of the tube. Coaxial tube (not shown) is in the center of the velocity field, into/out of the page. Length of arrow scales with fluid velocity magnitude.

To understand the potential benefit of convection, we evaluated convection results in comparison with conduction-only systems. We used a 1 mD reservoir to simulate conduction-only conditions. To ensure this was an accurate assumption, we compared our convection simulations at 1 mD with a hot dry rock conduction-only model presented in (White et al. 2024). Figure 3 shows good agreement between the hot dry rock model and our conduction assumption in the convection model for both outlet temperature and thermal energy. The slight difference between the two cases is due to the porosity of the hot wet rock of the convection model. The model still assumes a porosity of 10%, which means that our model assumes the pores are filled with water and uses an effective thermal conductivity to calculate temperature in the rock. We see a distinct spike in production temperature during the first year, which then decreases and steadies out over the course of the simulation time. Note that the system has not reached steady state after 20 years of operation in Figure 3.

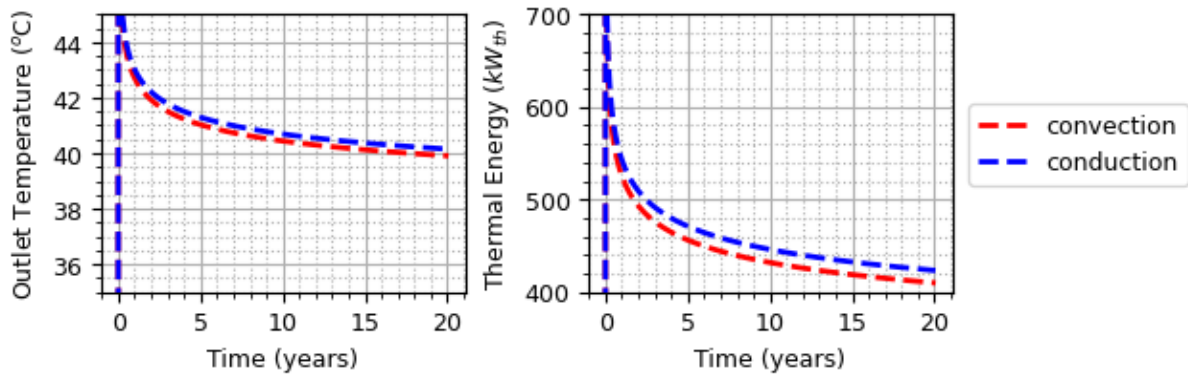


Figure 3: Comparison between L-shape coaxial with and without convection in the horizontal section with a mass flow rate of 10 kg/s, a permeability of 1 mD, and a temperature gradient of 30 °C/km.

Figure 4 compares the outlet water temperature for mass flow rates of 2 kg/s and 10 kg/s for a permeability of 1 D. Results show that the outlet temperature increases with decreasing mass flow rate. For a geothermal gradient of 30 °C/km, an outlet temperature of 64.5 °C is achieved for a mass flow rate of 2 kg/s. If the mass flow rate is increased to 10 kg/s, the outlet temperature decreases to 41.2 °C. A more significant temperature difference was observed for a geothermal temperature gradient of 90 °C/km when the mass flow rate is increased

from 2 kg/s to 10 kg/s. For a mass flow rate of 2 kg/s, the outlet temperature reaches 156.7 °C, more than double the outlet temperature reached for the geothermal temperature gradient of 30 °C/km. The outlet temperature for a mass flow rate of 10 kg/s decreases to 85.5 °C. To show the effect of convection, the outlet temperature for a permeability of 1 mD was also included in Figure 4, which represents the conduction case. No significant improvement was observed for the geothermal temperature gradient of 30 °C/km. On the other hand, having natural convection in the HWR increases the outlet temperature by 21.5 °C for a system with a geothermal temperature gradient of 90 °C/km for both mass flow rates.

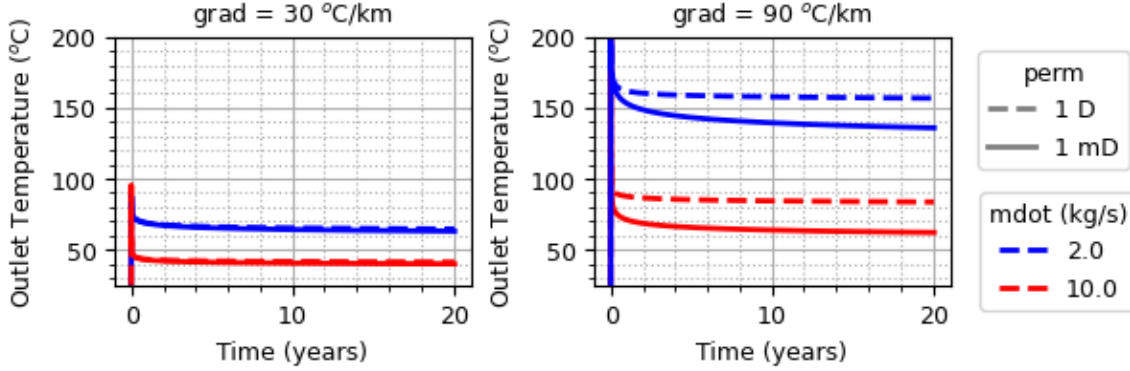


Figure 4: Comparison of outlet temperature for the L-shape coaxial geothermal system for two mass flow rates (2.0 kg/s and 10.0 kg/s). The horizontal section has a permeability of 1 D and a temperature gradient of 30 °C/km (left) and 90 °C/km (right). The conduction results (1 mD) are also shown for reference.

Thermal energy (Figure 5) shows a different trend from the outlet temperature results. The thermal energy increases with increasing mass flow rate. For a geothermal gradient of 30 °C/km, there is still a small increase in thermal energy when the mass flow rate increases from 2 kg/s to 10 kg/s and almost no advantage of having natural convection in the formation. However, if the geothermal temperature gradient is 90 °C/km, a much higher thermal energy is achieved for both mass flow rates. In addition, by increasing the mass flow rate from 2 kg/s to 10 kg/s, the thermal energy doubles. The only significant improvement on the thermal energy (60% increase) due to natural convection is for the geothermal temperature gradient is 90 °C/km and mass flow rate of 10 kg/s.

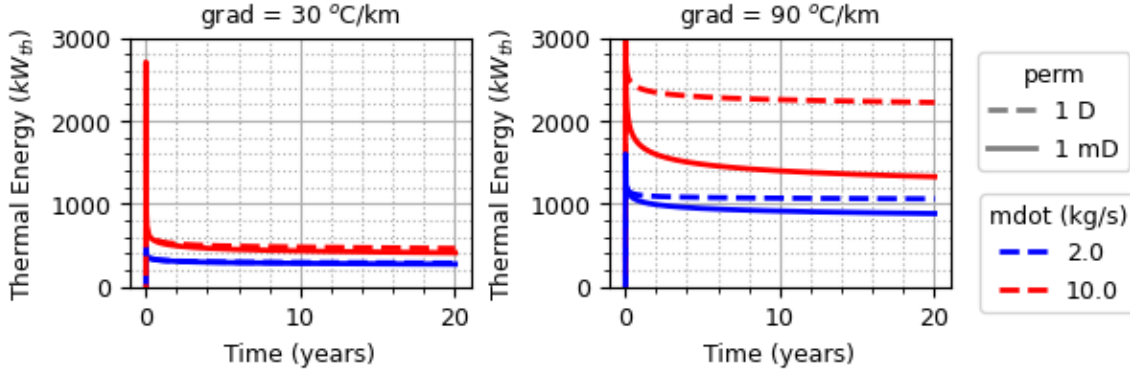


Figure 5: Comparison of thermal energy for the L-shape coaxial geothermal system for two mass flow rates (2.0 kg/s and 10.0 kg/s). The horizontal section has a permeability of 1 D and a temperature gradient of 30 °C/km (left) and 90 °C/km (right). The conduction results (1 mD) are also shown for reference.

Figure 6 compares the outlet temperature for the three geothermal gradients (30 °C/km, 60 °C/km, and 90 °C/km). As expected, the higher the geothermal temperature gradient is, the higher the outlet temperature is. There is no advantage of having natural convection in the formation for a 30 °C/km geothermal temperature gradient. However, as the temperature gradient increases, the effect of natural convection on the outlet temperature also increase. This is true for both mass flow rates, but a more significant temperature increase is observed for the lower mass flow rate (2 kg/s). If we are more interested in the thermal energy and not the outlet temperature, then a higher mass flow rate will result in a higher thermal energy as shown in Figure 7.

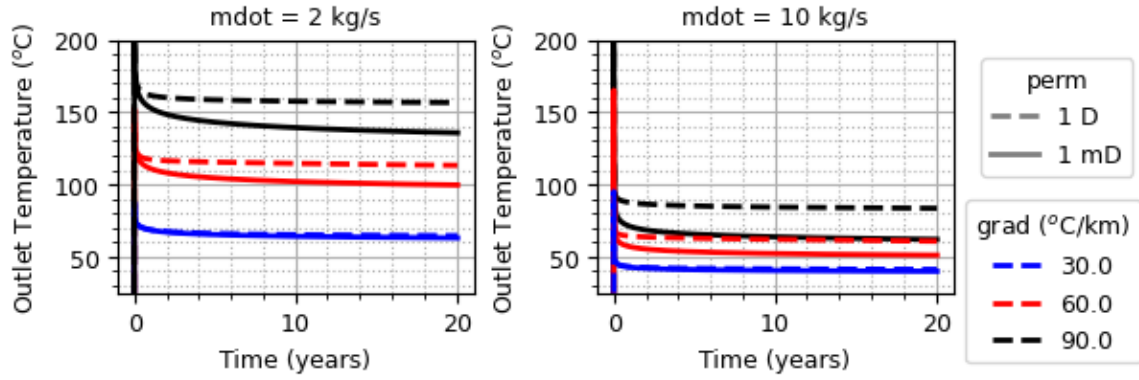


Figure 6: Comparison of outlet temperature for the L-shape coaxial geothermal system for three temperature gradients ($30 \text{ }^{\circ}\text{C}/\text{km}$, $60 \text{ }^{\circ}\text{C}/\text{km}$, and $90 \text{ }^{\circ}\text{C}/\text{km}$). The horizontal section has a permeability of 1 D and a mass flow rate of 2 kg/s (left) and 10 kg/s (right). The conduction results (1 mD) are also shown for reference.

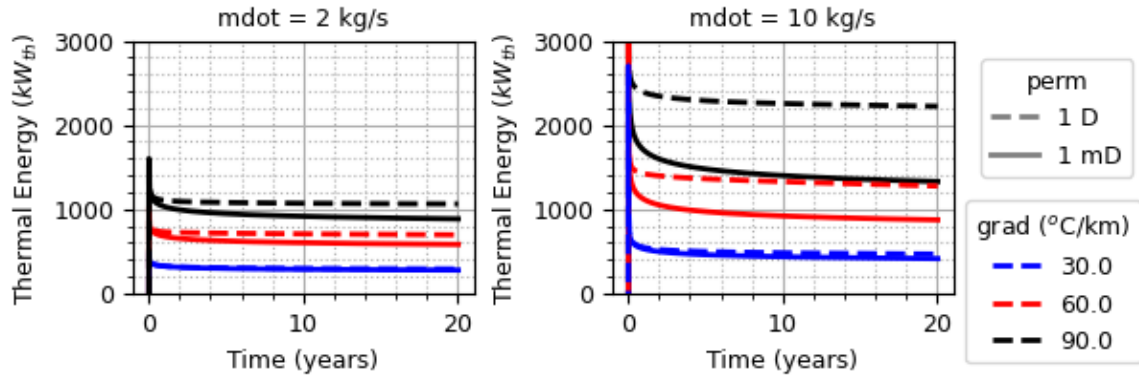


Figure 7: Comparison of thermal energy for the L-shape coaxial geothermal system for three temperature gradients ($30 \text{ }^{\circ}\text{C}/\text{km}$, $60 \text{ }^{\circ}\text{C}/\text{km}$, and $90 \text{ }^{\circ}\text{C}/\text{km}$). The horizontal section has a permeability of 1 D and a mass flow rate of 2 kg/s (left) and 10 kg/s (right). The conduction results (1 mD) are also shown for reference.

Lastly, we compare the outlet temperature (Figure 8) and the thermal energy (Figure 9) for six different permeabilities ranging from 1 mD (conduction case) to 5 D using a thermal gradient of $30 \text{ }^{\circ}\text{C}/\text{km}$. The increase in permeability from 1 mD to 5 D only increases the outlet temperature at 20 years of operation by $7 \text{ }^{\circ}\text{C}$ for a mass flow rate of 2 kg/s and $5 \text{ }^{\circ}\text{C}$ for a mass flow rate of 10 kg/s . A higher permeability would be needed to have a significant advantage for having convection in the formation. We observed a more significant impact on the thermal energy for 10 kg/s . The thermal energy increases from $409.8 \text{ kW}_{\text{th}}$ to $616.9 \text{ kW}_{\text{th}}$. However, a $207 \text{ kW}_{\text{th}}$ might still be a relatively low advantage for an increase in permeability to 5 D, a relatively unrealistic scenario.

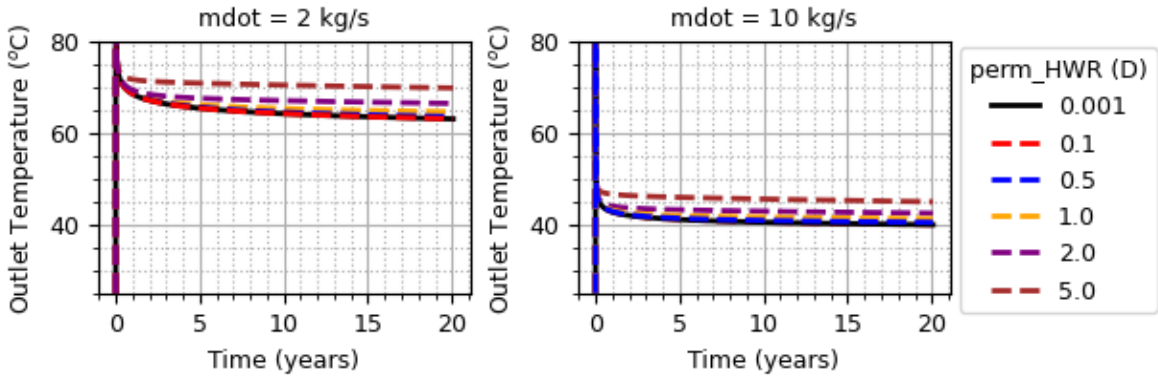


Figure 8: Comparison of outlet temperature for the L-shape coaxial geothermal system for different permeabilities ranging from 1 mD to 5 D. The system has a temperature gradient of $30 \text{ }^{\circ}\text{C}/\text{km}$ and a mass flow rate of 2 kg/s (left) and 10 kg/s (right).

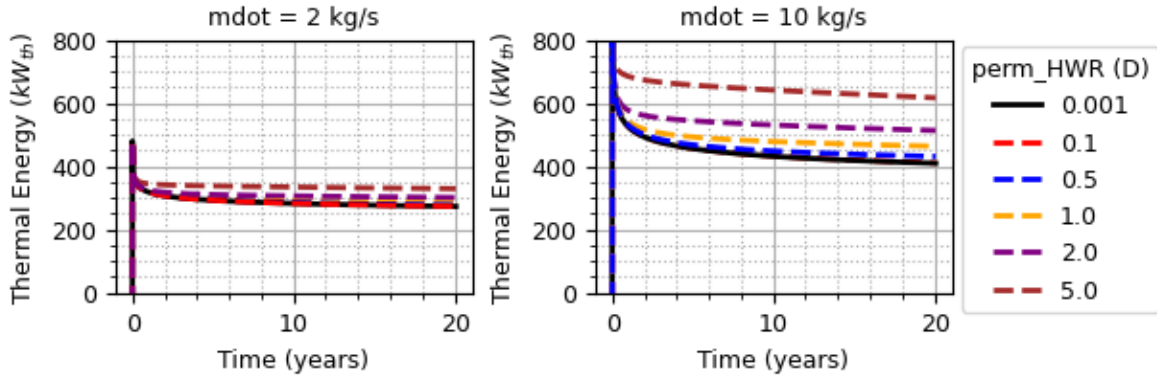


Figure 9: Comparison of thermal energy for the L-shape coaxial geothermal system for different permeabilities ranging from 1 mD to 5 D. The system has a temperature gradient of 30 °C/km and a mass flow rate of 2 kg/s (left) and 10 kg/s (right).

3.2 Comparison of Coaxial and U-tube systems

Here, we compare the outlet temperature (see Figure 10) and the thermal energy (see Figure 11) of the L-shape coaxial system with the U-tube system to determine which system results in greater outlet temperature and thermal energy. Note that Figure 10 uses an updated U-tube model solving the equations described in Section 2.3, while Figure 11 uses values directly from (Hakes et al. 2024). The U-tube system performs slightly better than the L-shape coaxial system. The U-tube outlet temperature at 20 years of operation is 5.7 °C higher than the coaxial system output temperature. Both systems show a small increase in temperature from the conduction-only case. The U-tube outlet temperature increases only 1 °C, and the coaxial outlet temperature increases only 2 °C as the permeability is increased from 1 mD to 1 D. The thermal energy at 20 years of operation of the U-tube system is 229.4 kW_{th} higher than the thermal energy of the coaxial system. Natural convection also improves slightly the thermal energy. A techno-economic analysis should be performed to determine whether the higher performance of the U-tube system outweighs the extra vertical drilling cost.

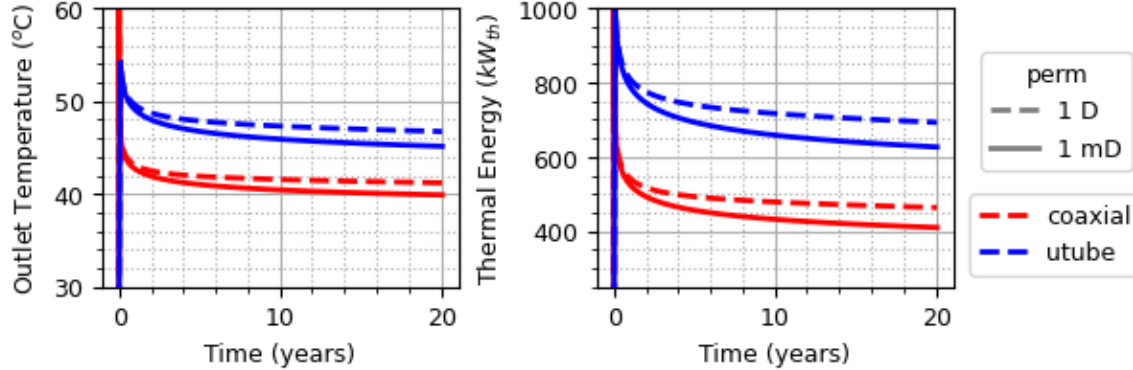


Figure 10: Comparison between L-shape coaxial and U-tube shape both with natural convection in the horizontal section with a mass flow rate of 10 kg/s, a permeability of 1 D, and a temperature gradient of 30 °C/km.

Finally, in Figure 11, we compare the impact of convection on the steady 20-year heat output (i.e. thermal energy) of the well for varying permeability and the two mass flow rates. The conduction only case (1 mD) was also included to indicate the potential benefit of convection as permeability increases. At low permeability, there is no increase in heat output over conduction for both the coaxial and the U-tube systems. At 500 mD, there is a low increase (<5% increase in heat output). At 1 D and above, heat output increases with increasing permeability. The higher mass flow rate of 10 kg/s increases the impact of convection over conduction on heat output. Surprisingly, there is a higher increase in heat output for the coaxial system compared to the U-tube system for both mass flow rates. However, from Figure 10, we see that even with the higher increase in outlet temperature or thermal energy, the coaxial system is not able to reach the higher values from the U-tube system.

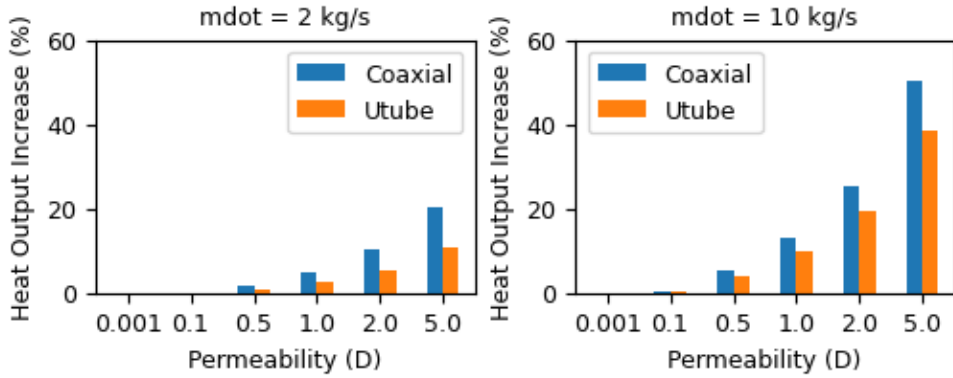


Figure 11: Increase in heat output at 20 years due to natural convection versus the heat conduction-only scenario for a permeability of 1 mD to 5 D. The geothermal temperature gradient is 30 °C/km.

4. SUMMARY

Table 2 summarizes the results in Section 3.1 and Section 3.2. The table presents the outlet temperature and thermal energy at 20 years of operation for different mass flow rates, geothermal temperature gradients, and permeabilities. The results from the U-tube system used in Section 3.2 were also included in the table.

Table 2: Summary of the outlet temperature and thermal energy at 20 years of operation of the coaxial system for different mass flow rates, geothermal temperature gradients, and permeabilities, and the U-tube system.

System	Mass flow rate (kg/s)	Temperature gradient (°C /km)	permeability (D)	Outlet temperature (°C)	Thermal energy (kWth)
Coaxial	2	30	0.001	63.0	273.3
	2	30	0.1	63.0	273.5
	2	30	0.5	63.5	277.5
	2	30	1	64.5	286.1
	2	30	2	66.4	301.4
	2	30	5	69.7	329.4
	2	60	0.001	99.6	578.6
	2	60	1	113.2	692.5
	2	90	0.001	135.7	882.4
	2	90	1	156.7	1060.1
	10	30	0.001	39.9	409.8
	10	30	0.1	39.9	411.0
	10	30	0.5	40.4	431.4
	10	30	1	41.2	463.5
	10	30	2	42.4	513.5
	10	30	5	44.9	616.9
	10	60	0.001	51.0	870.5
	10	60	1	60.7	1273.0
	10	90	0.001	62.0	1326.1
	10	90	1	83.5	2221.1
U-tube	10	30	0.001	45.1	626.6
	10	30	1	46.7	692.9

5. CONCLUSIONS

Similar to the results found for U-tube systems, we find that higher geothermal gradients and higher permeability results in increased impacts from natural convection. Outlet temperature and thermal energy were found to increase more significantly with temperature for higher permeabilities (1 D and above); however, typical permeabilities at 2 km depth in the continental crust are on the order of 1 mD, a condition found to be nearly equivalent to a conduction-only reservoir. We found that lower mass flow rates result in higher output temperatures but also result in lower thermal energy. An optimization needs to be performed to find the mass flow rate that will optimize the outlet temperature and the thermal energy. In comparing coaxial and U-tube systems, the U-tube system outperforms the coaxial system for the specific conditions we modeled. We also found a higher percentage increase in heat output for the coaxial system compared to the U-tube system for both mass flow rates. However, the higher percentage increase that can be observed in the coaxial system is not enough to reach the values from the U-tube system. The coaxial system might be able to outperform the U-tube system at higher mass flow rates, higher permeabilities, or higher geothermal temperature gradients. These higher values, however, might not be realistic.

ACKNOWLEDGEMENTS

The authors would like to acknowledge Victor Brunini and Yaro Vasyliv for discussions on model development. Funding provided by the U.S. Department of Energy Office of Energy Efficiency and Renewable Energy Geothermal Technologies Office. Sandia National Laboratories is a multimission laboratory managed and operated by National Technology and Engineering Solutions of Sandia, LLC., a wholly owned subsidiary of Honeywell International, Inc., for the U.S. Department of Energy National Nuclear Security Administration under contract DE-NA0003525. This work was authored in part by the National Renewable Energy Laboratory, operated by Alliance for Sustainable Energy, LLC, for the U.S. Department of Energy (DOE) under Contract No. DE-AC36-08GO28308. This paper describes objective technical results and analysis. Any subjective views or opinions that might be expressed in this paper do not necessarily represent the views of the U.S. Department of Energy or the United States Government. The U.S. Government retains and the publisher, by accepting the article for publication, acknowledges that the U.S. Government retains a nonexclusive, paid-up, irrevocable, worldwide license to publish or reproduce the published form of this work, or allow others to do so, for U.S. Government purposes.

6. REFERENCES

- Aljubran, Mohammad J, and Roland N Horne. 2025. 'Techno-economics of geothermal power in the contiguous United States under baseload and flexible operations', *Renewable and Sustainable Energy Reviews*, 211: 115322.
- Beckers, Koenraad, Adam Ketchum, and Chad Augustine. 2024. "Evaluating Heat Extraction Performance of Closed-Loop Geothermal Systems with Thermally Conductive Enhancements in Conduction-Only Reservoirs." In.: National Renewable Energy Laboratory (NREL), Golden, CO (United States).
- Beckers, Koenraad, Yaroslav Vasyliv, Gabriela A Bran-Anleu, Mario Martinez, Chad Augustine, and Mark White. 2023. "Tabulated Database of Closed-Loop Geothermal Systems Performance for Cloud-Based Technical and Economic Modeling of Heat Production and Electricity Generation." In.: National Renewable Energy Lab.(NREL), Golden, CO (United States).
- Bell, Ian H, Jorrit Wronski, Sylvain Quoilin, and Vincent Lemort. 2014. 'Pure and pseudo-pure fluid thermophysical property evaluation and the open-source thermophysical property library CoolProp', *Industrial & engineering chemistry research*, 53: 2498-508.
- Hakes, Raquel S.P., Radoslav Bozinoski, Koenraad F. Beckers, and Adam Ketchum. 2024. "Influence of Reservoir Convection on Heat Extraction with Closed-Loop Geothermal Systems." In *Geothermal Rising Conference (GRC)*. Waikoloa, HI, USA: GRC Transaction.
- Incropera, Frank P, David P DeWitt, Theodore L Bergman, and Adrienne S Lavine. 1996. *Fundamentals of heat and mass transfer* (Wiley New York).
- Munson, Bruce Roy, Donald F Young, and Theodore Hisao Okiishi. 1995. 'Fundamentals of fluid mechanics', *Oceanographic Literature Review*, 10: 831.
- "SIERRA Multimechanics Module: Aria User Manual (V.5.6)." In. 2022. Medium: ED; Size: 5190 p. United States.
- White, Mark, Yaroslav Vasyliv, Koenraad Beckers, Mario Martinez, Paolo Balestra, Carlo Parisi, Chad Augustine, Gabriela Bran-Anleu, Roland Horne, and Laura Pauley. 2024. 'Numerical investigation of closed-loop geothermal systems in deep geothermal reservoirs', *Geothermics*, 116: 102852.